Supporting Information

Ultrafast Preparation of Ruthenium Nanoparticle/Molybdenum Oxide/Nitrogen-Doped Carbon Nanocomposites by Magnetic Induction Heating for Efficient Hydrogen Evolution Reaction

Bingzhe Yu,[a] Qiming Liu,[a] Dingjie Pan,[a] Kevin Singewald,[a] Davida DuBois,[a] John Tressel,[a] Bryan Hou,[a] Glenn L. Millhauser,[a] Frank Bridges,[b] and Shaowei Chen[a,*]

[a] Department of Chemistry and Biochemistry, University of California, 1156 High Street, Santa Cruz, CA 95064, United States
[b] Department of Physics, University of California, 1156 High Street, Santa Cruz, CA 95064, United States
* E-mail: shaowei@ucsc.edu

List of Contents
- 31 figures
- 8 tables
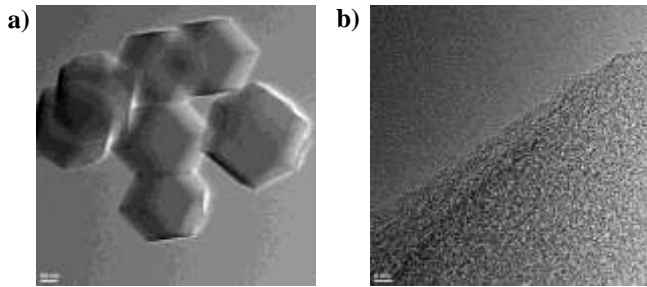
Figure S1. TEM images of MoO$_x$/NC. Scale bars are (a) 50 nm and (b) 5 nm.
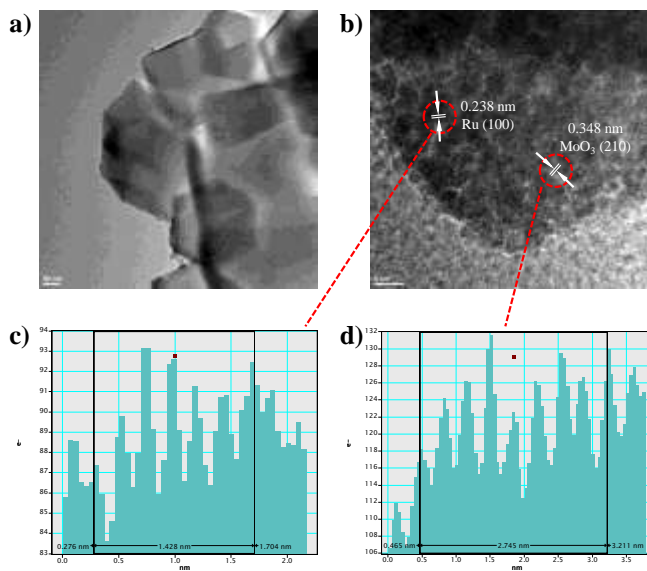

Figure S2. (a,b) TEM images of RuMoO$_x$/NC-1. Scale bars are (a) 50 nm and (b) 5 nm. The interplanar spacing of the lattice fringes for (c) Ru (100) and (d) MoO$_3$ (210) of the circled areas in panel (b).
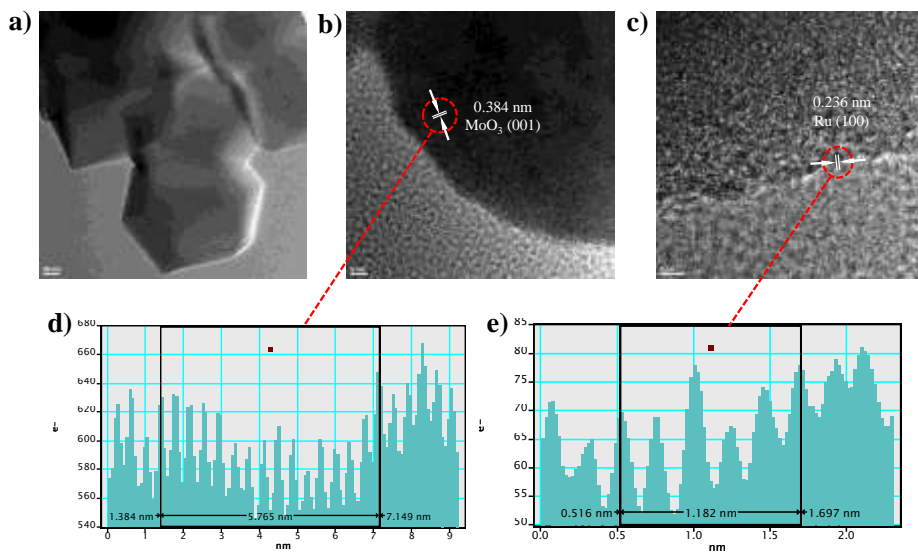

Figure S3. (a-c) TEM images of RuMoO$_x$/NC-2. Scale bars are (a) 50 nm, (b) 5 nm and (c) 2 nm. The interplanar spacing of the lattice fringes for (d) MoO$_3$ (001) and (e) Ru (100) of the circled areas in panel (b) and (c), respectively.
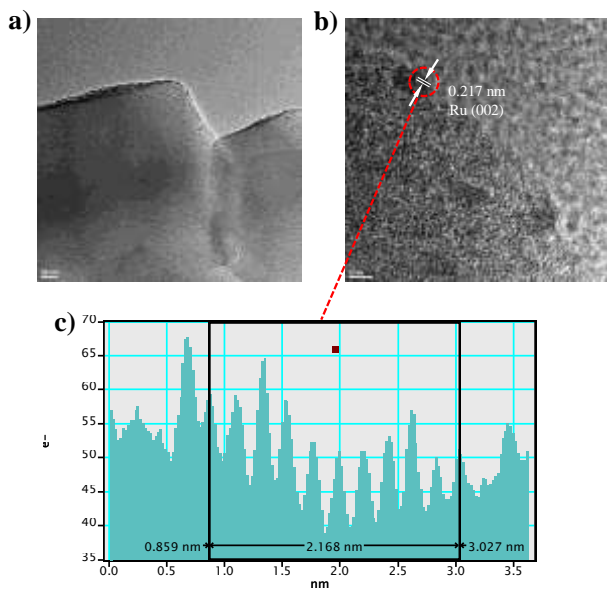
Figure S4. (a,b) TEM images of RuMoO$_x$/NC-3. Scale bars are (a) 20 nm and (b) 2 nm. The interplanar spacing of the lattice fringes for (c) Ru (002) of the circled area in panel (b).
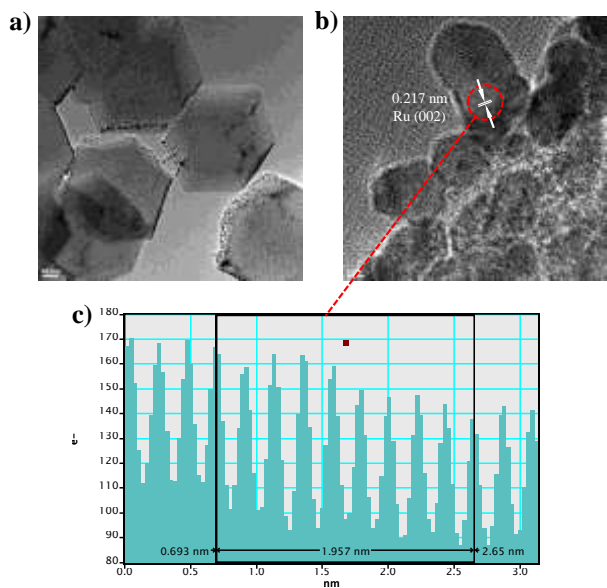
Figure S5. (a,b) TEM images of RuMoO$_x$/NC-4. Scale bars are (a) 50 nm and (b) 2 nm. The interplanar spacing of the lattice fringes for (c) Ru (002) of the circled area in panel (b).
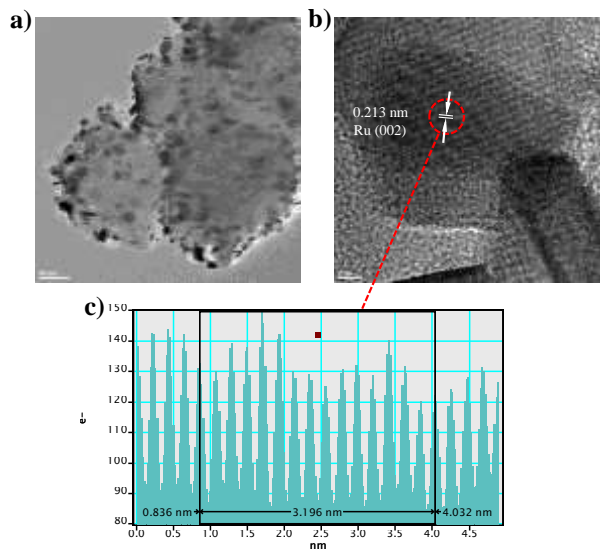
Figure S6. (a,b) TEM images of Ru/NC. Scale bars are (a) 50 nm and (b) 2 nm. The interplanar spacing of the lattice fringes for (c) Ru (002) of the circled area in panel (b).
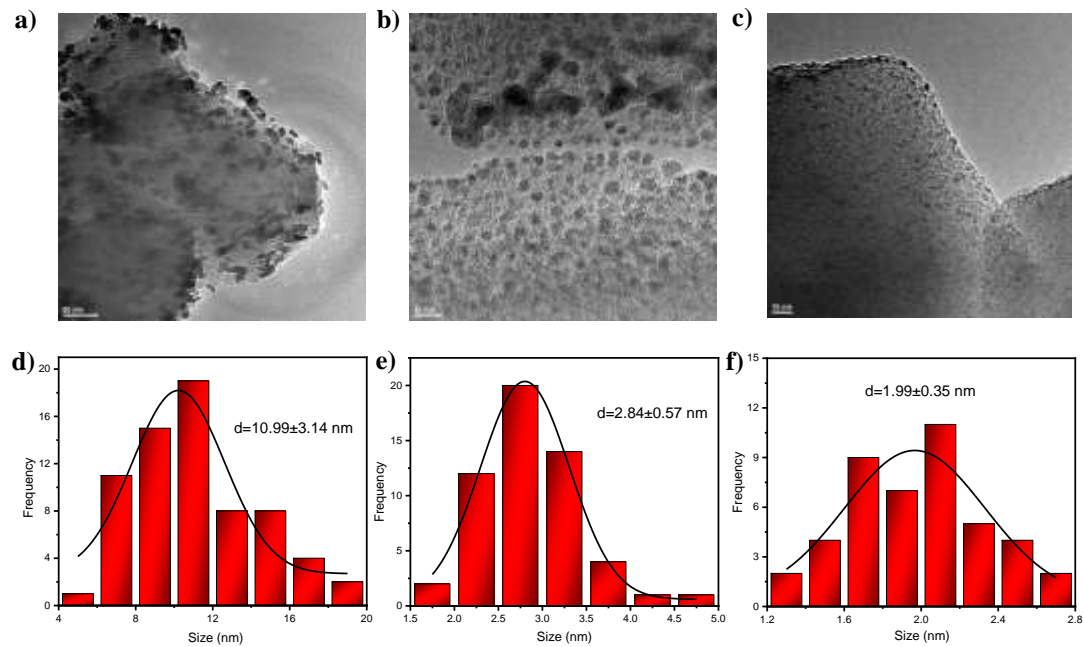
**Figure S7.** TEM images of (a) Ru/NC, (b) RuMoO$_x$/NC-4 and (c) RuMoO$_x$/NC-3. Scale bars are (a) 50 nm, (b) 10 nm and (c) 10 nm. (d-f) Particle size distribution histograms for (a-c), respectively.
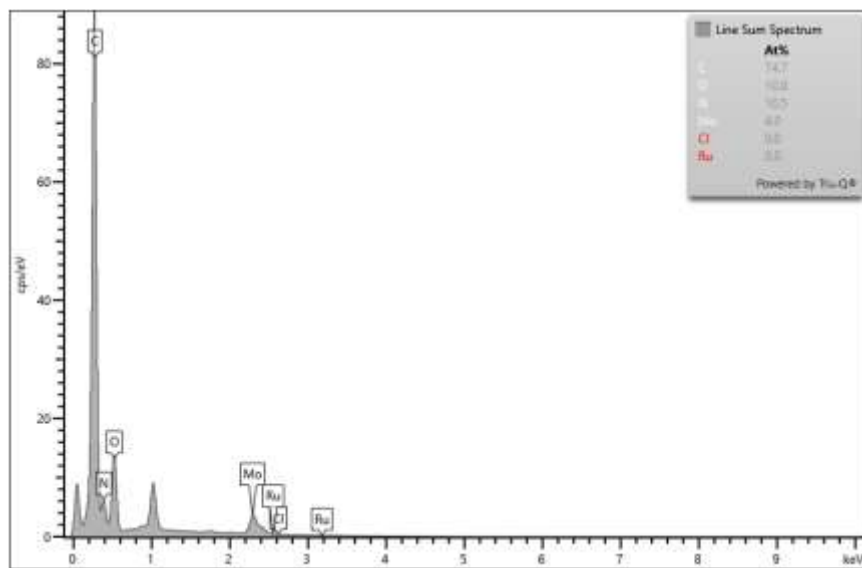
Figure S8. EDS plot of MoO$_x$/NC. Inset shows the elemental composition (at%).
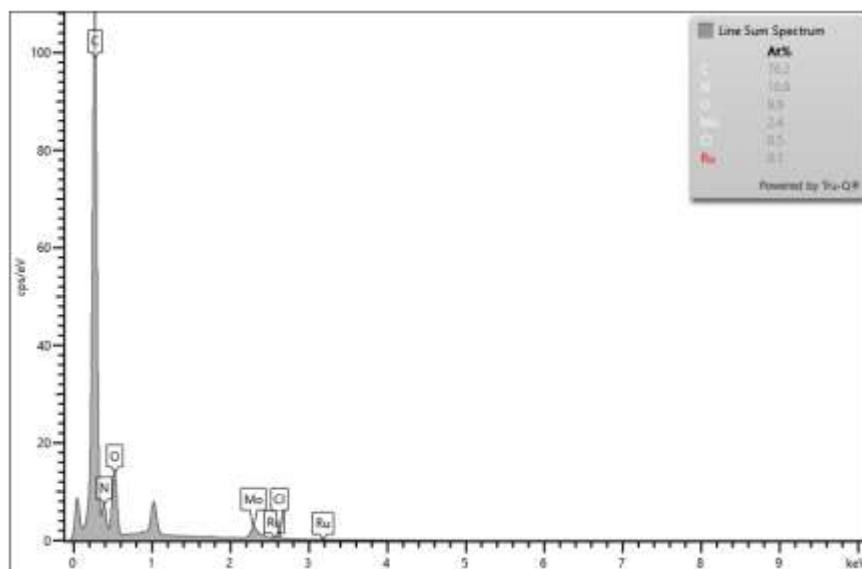
Figure S9. EDS plot of RuMoO$_x$/NC-1. Inset shows the elemental composition (at%).
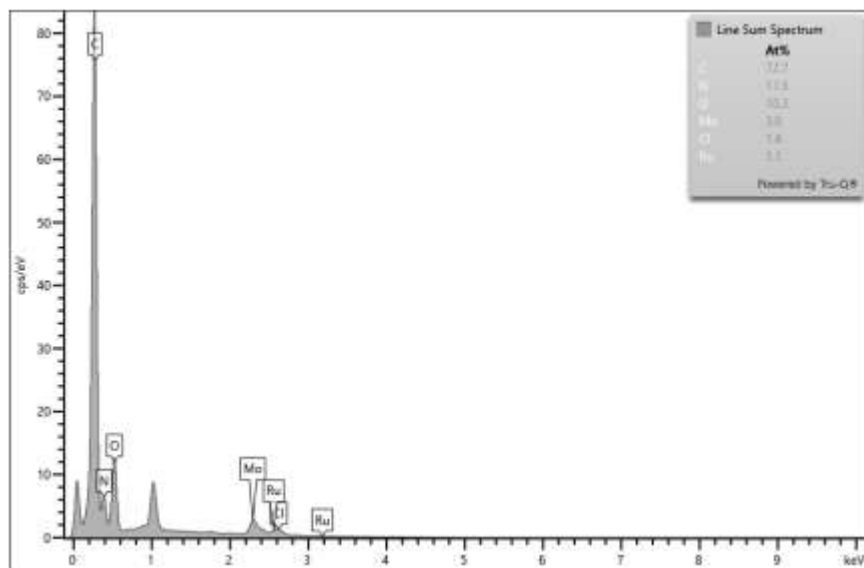
Figure S10. EDS plot of RuMoO$_x$/NC-2. Inset shows the elemental composition (at%).
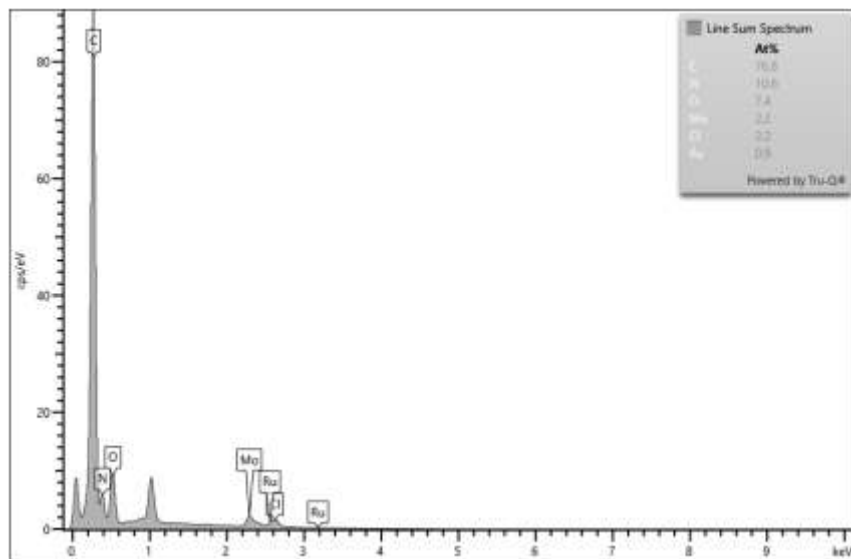
Figure S11. EDS plot of RuMoO$_x$/NC-3. Inset shows the elemental composition (at%).
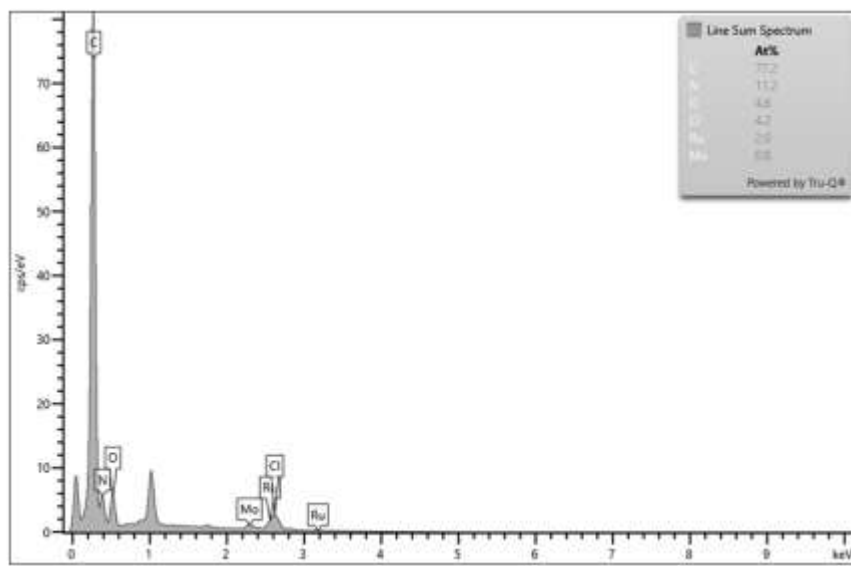
Figure S12. EDS plot of RuMoO$_x$/NC-4. Inset shows the elemental composition (at%).
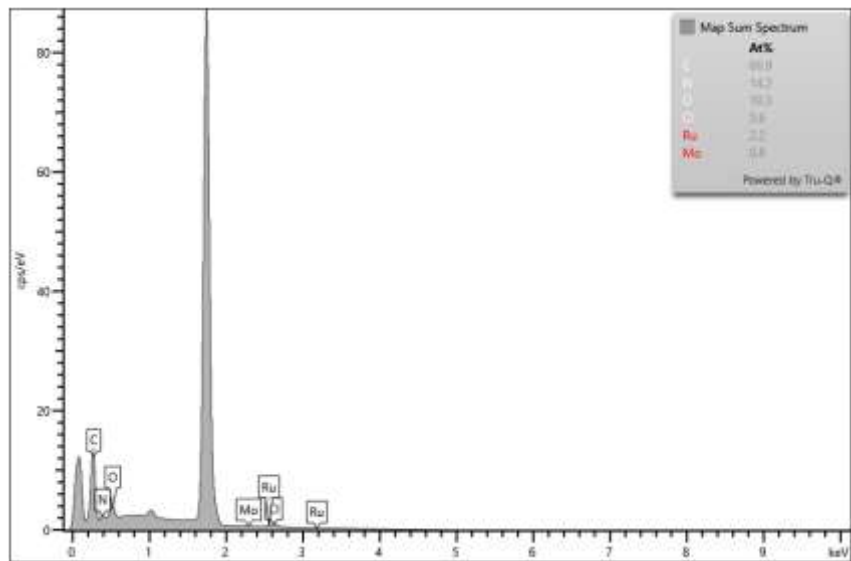
Figure S13. EDS plot of RuMoO$_x$/NC-5. Inset shows the elemental composition (at%).

	At%
C	76.3
N	9.9
Cl	4.8
Ru	3.0
O	2.6
Zn	2.5
Si	0.9
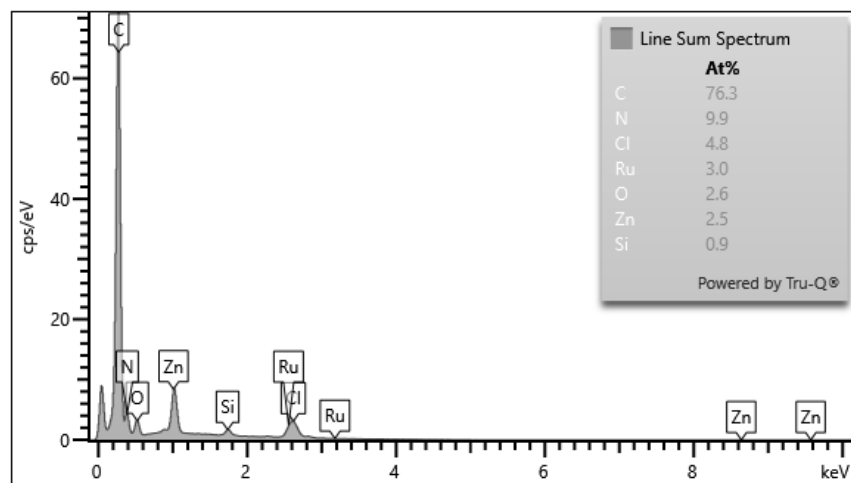
Figure S14. EDS plot of Ru/NC. Inset shows the elemental composition (at%).
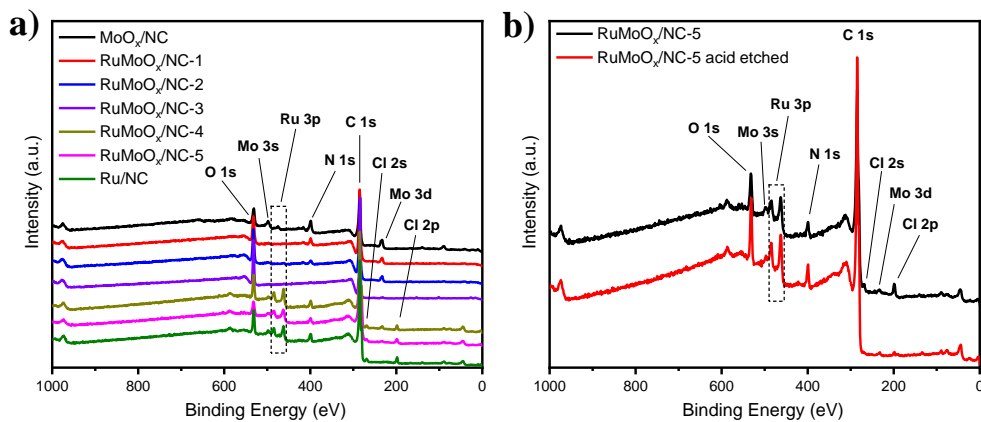
Figure S15. XPS survey spectra of (a) MoO$_x$/NC, RuMoO$_x$/NC-1, RuMoO$_x$/NC-2, RuMoO$_x$/NC-3, RuMoO$_x$/NC-4, RuMoO$_x$/NC-5 and Ru/NC; and (b) RuMoO$_x$/NC-5 and RuMoO$_x$/NC-5 acid etched.
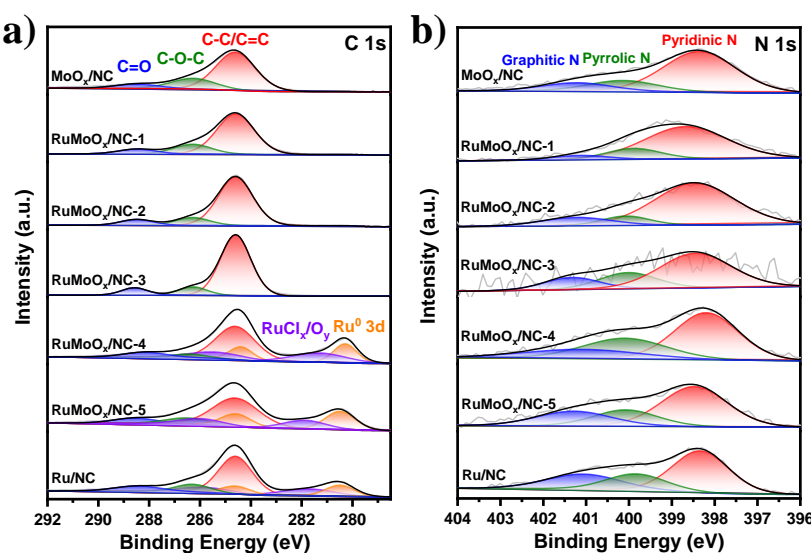
Figure S16. High-resolution XPS spectra of the (a) C 1s and (b) N 1s electrons of MoO$_x$/NC, RuMoO$_x$/NC-1, RuMoO$_x$/NC-2, RuMoO$_x$/NC-3, RuMoO$_x$/NC-4, RuMoO$_x$/NC-5 and Ru/NC.
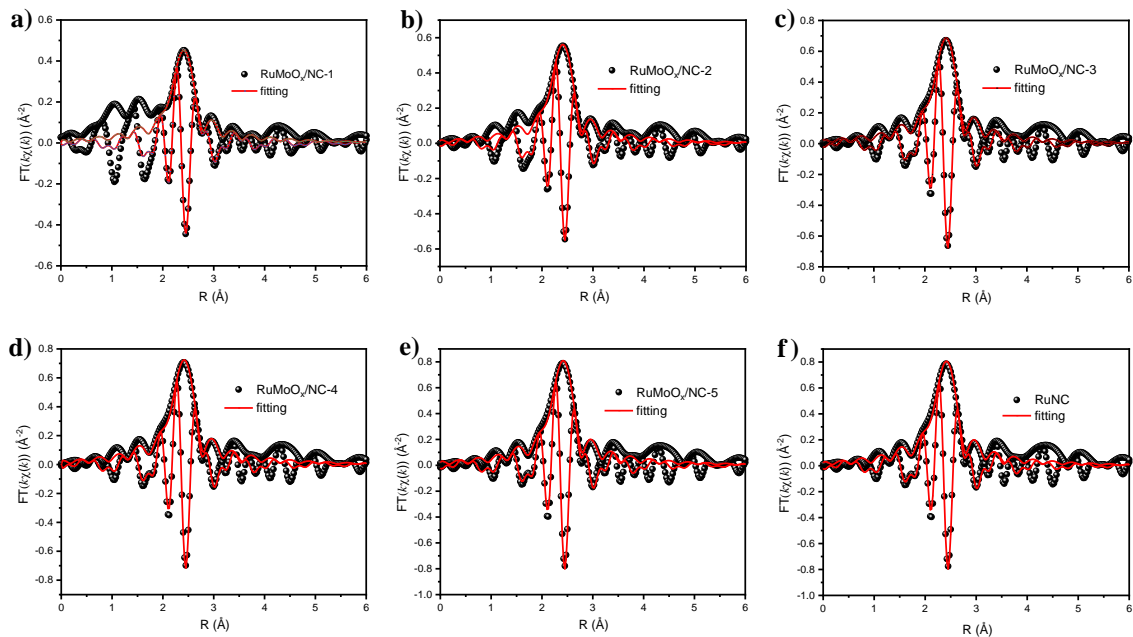
Figure S17. Fittings of Ru K-edge EXAFS of (a) RuMoO$_x$/NC-1, (b) RuMoO$_x$/NC-2, (c) RuMoO$_x$/NC-3, (d) RuMoO$_x$/NC-4, (e) RuMoO$_x$/NC-5, and (f) Ru/NC. Fit range is 2.0-2.8 Å.
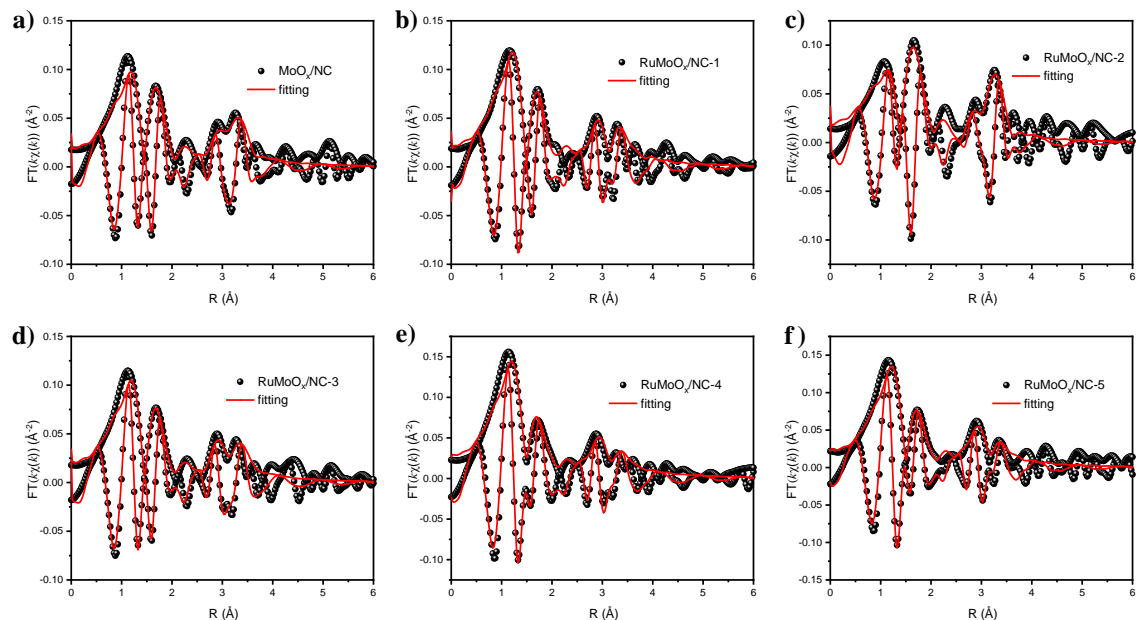
Figure S18. Fittings of Mo K-edge EXAFS of (a) MoO$_x$/NC, (b) RuMoO$_x$/NC-1, (c) RuMoO$_x$/NC-2, (d) RuMoO$_x$/NC-3, (e) RuMoO$_x$/NC-4, and (f) RuMoO$_x$/NC-5. Fit range is 0.8-3.5 Å.
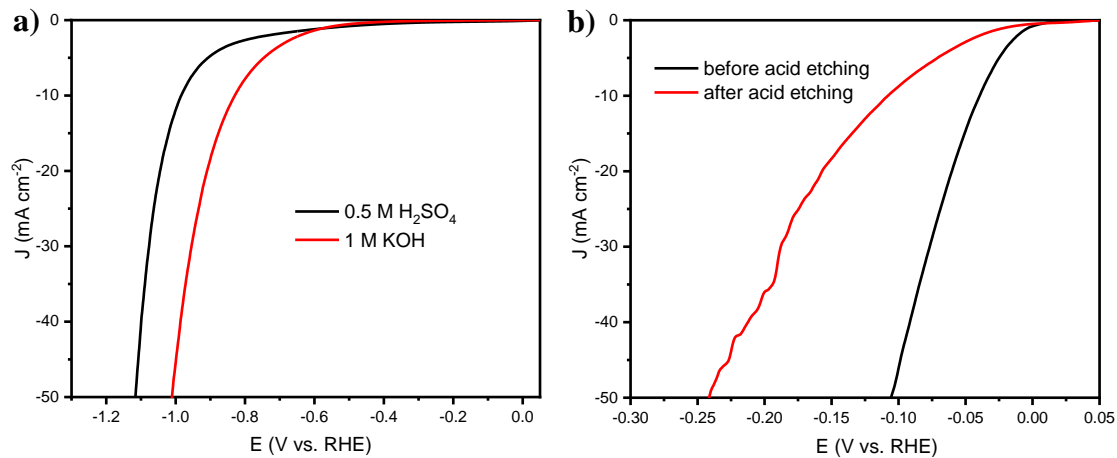
Figure S19. (a) HER polarization curves of NC in 0.5 M H_2SO_4 and 1 M KOH. (b) HER polarization curves of RuMoO$_x$/NC-5 in 1 M KOH before and after treatment in a 4 M H_3PO_4 solution.
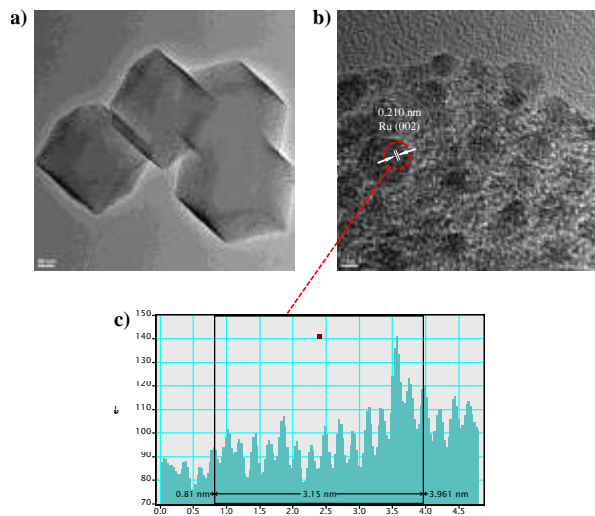
Figure S20. (a,b) TEM images of RuMoO$_x$/NC-5 after acid etching. Scale bars are (a) 50 nm and (b) 2 nm. The interplanar spacing of the lattice fringes for (c) Ru (002) of the circled area in panel (b).
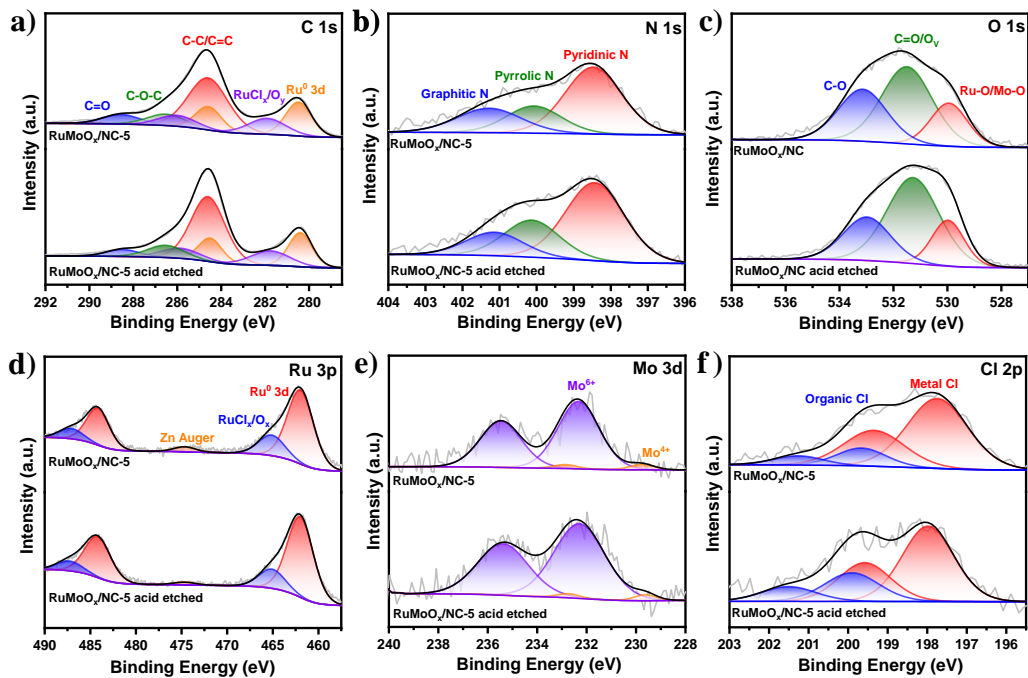
Figure S21. High-resolution XPS spectra of (a) C 1s, (b) N 1s, (c) O 1s, (d) Ru 3p, (e) Mo 3d, and (f) Cl 2p for RuMoO$_x$/NC-5 and RuMoO$_x$/NC-5 acid etched.
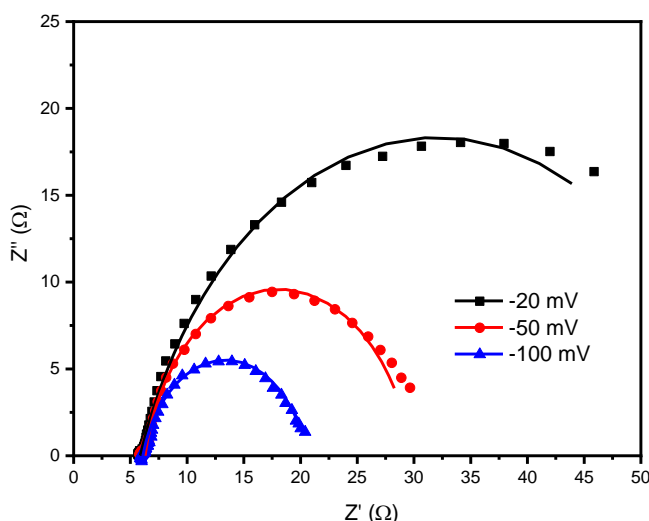
Figure S22. Nyquist plots of RuMoO$_x$/NC-5 at the overpotential of -20 mV, -50 mV and -100 mV in 1 M KOH.
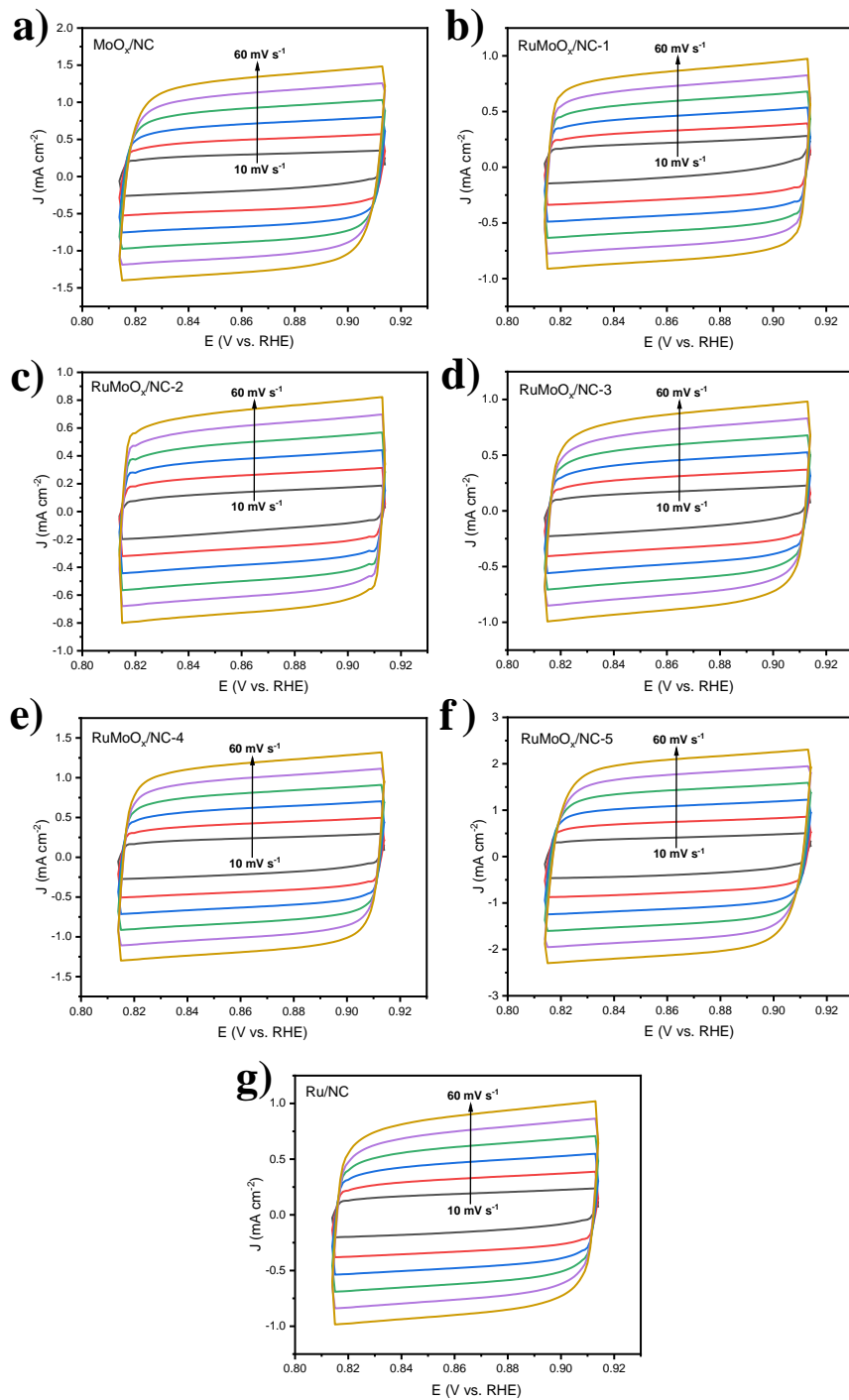
Figure S23. Cyclic Voltammograms of (a) MoO$_x$/NC, (b) RuMoO$_x$/NC-1, (c) RuMoO$_x$/NC-2, (d) RuMoO$_x$/NC-3, (e) RuMoO$_x$/NC-4, (f) RuMoO$_x$/NC-5, and (g) Ru/NC within the range of +0.814 to +0.914 V at various scan rates in 1 M KOH.
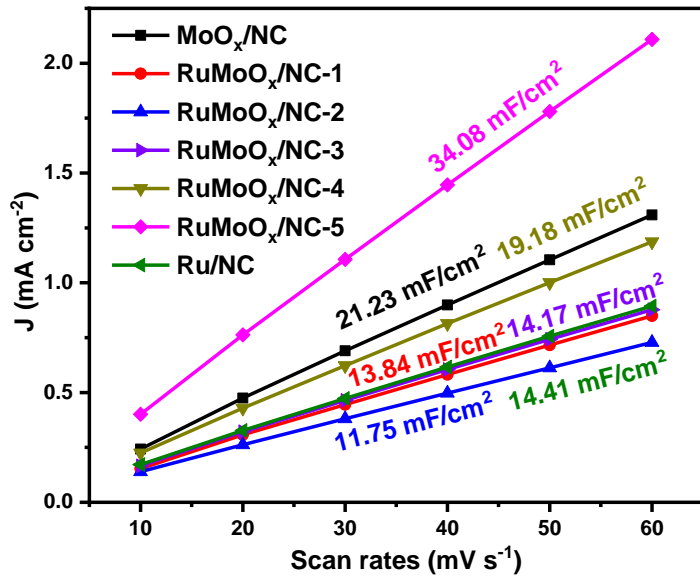
Figure S24. Variation of the double-layer charging current at +0.864 V with scan rate of MoO$_x$/NC, RuMoO$_x$/NC-1, RuMoO$_x$/NC-2, RuMoO$_x$/NC-3, RuMoO$_x$/NC-4, RuMoO$_x$/NC-5, Ru/NC and 20 wt% Pt/C in 1 M KOH, from which the double-layer capacitance (C$_{dl}$) is estimated.
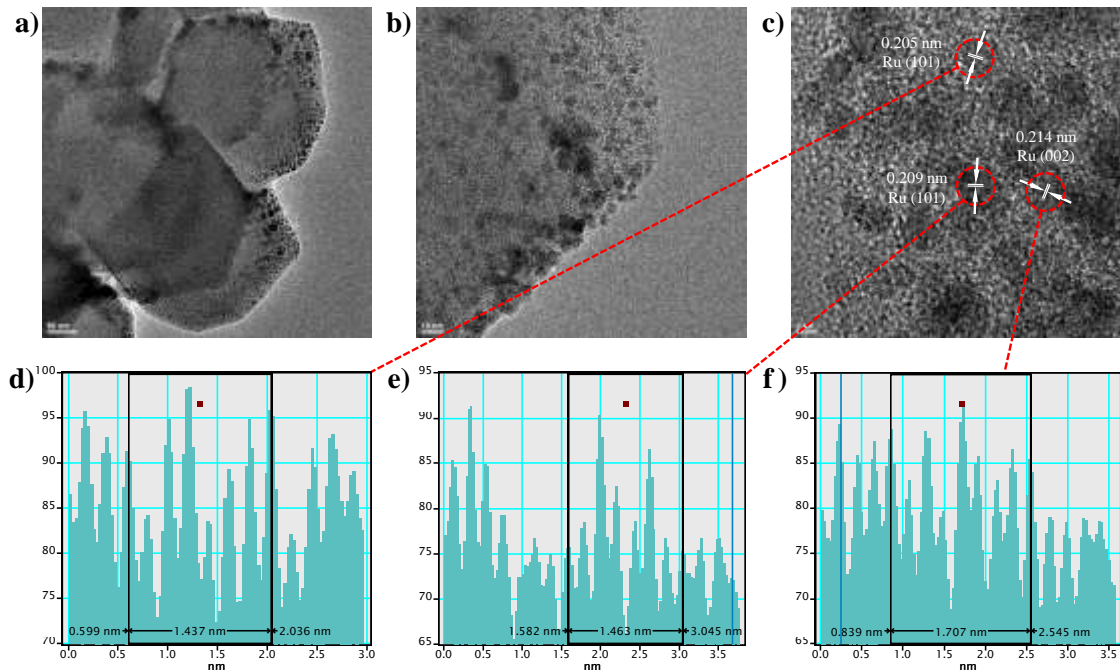
Figure S25. (a,b,c) TEM images of RuMoO$_x$/NC-5 after 5000 CV cycles. Scale bars are (a) 50 nm, (b) 10 nm and (c) 2 nm. The interplanar spacing of the lattice fringes of the circled areas in panel (c) are shown in panels (d,e) Ru (101) and (f) Ru (002).
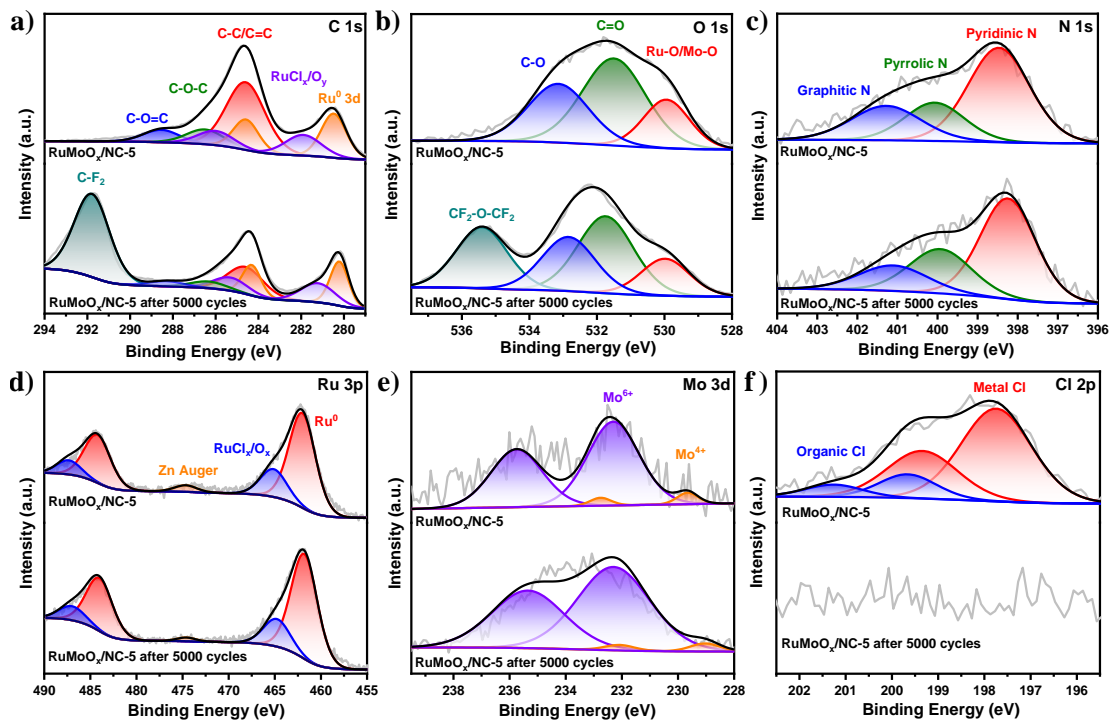
Figure S26. High-resolution XPS scans of (a) the C 1s, (b) O 1s, (c) N 1s, (d) Ru 3p, (e) Mo 3d, and (f) Cl 2p electrobs for RuMoO$_x$/NC-5 and RuMoO$_x$/NC-5 after 5000 CV cycles.
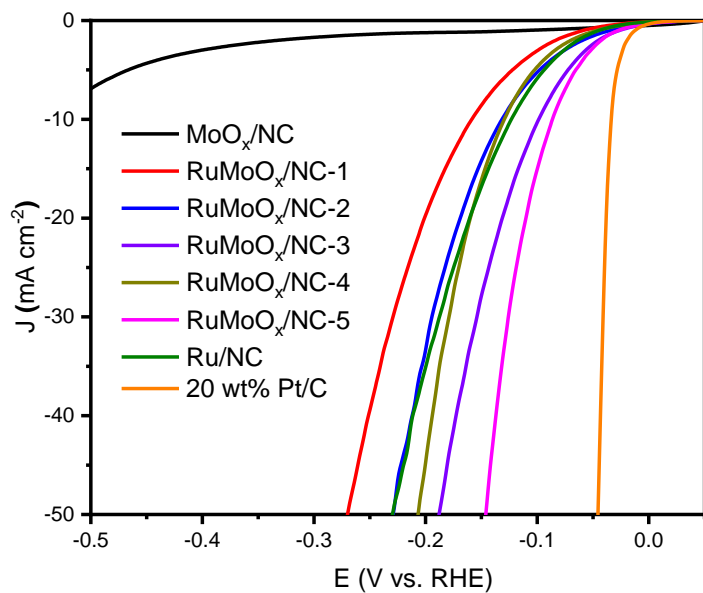
Figure S27. HER polarization curves in 0.5 M H$_2$SO$_4$ of MoO$_x$/NC, RuMoO$_x$/NC-1, RuMoO$_x$/NC-2, RuMoO$_x$/NC-3, RuMoO$_x$/NC-4, RuMoO$_x$/NC-5, Ru/NC and 20 wt% Pt/C.
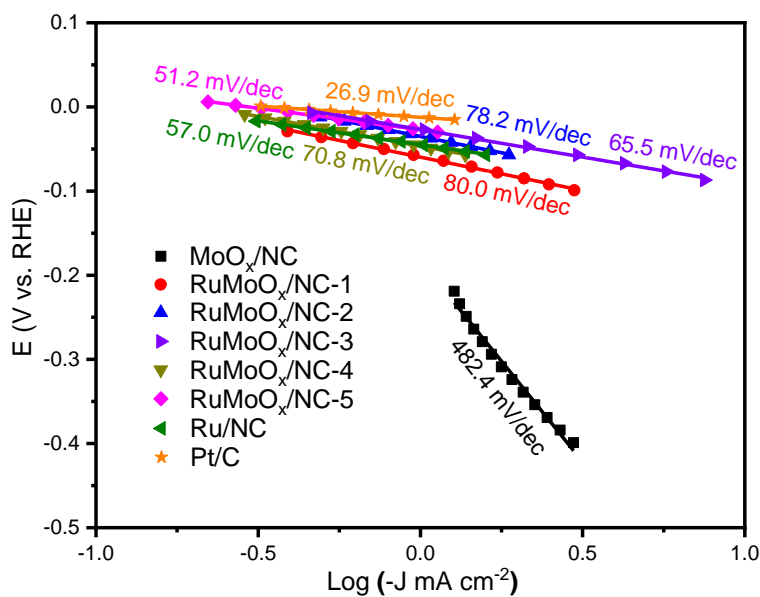
Figure S28. Tafel plots of MoO$_x$/NC, RuMoO$_x$/NC-1, RuMoO$_x$/NC-2, RuMoO$_x$/NC-3, RuMoO$_x$/NC-4, RuMoO$_x$/NC-5, Ru/NC and 20 wt% Pt/C in 0.5 M H$_2$SO$_4$.
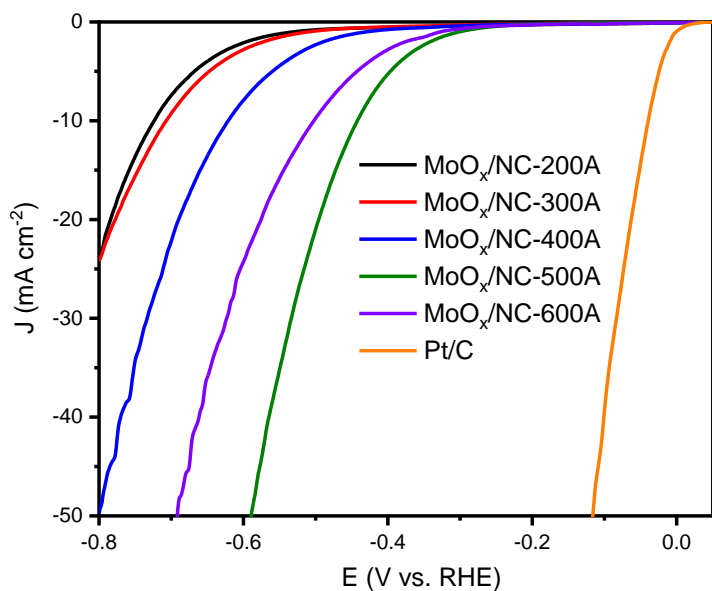
Figure S29. HER polarization curves of MoO$_x$/NC composites prepared by MIH at currents varied from 200 A to 600 A for 10 s (i.e., MoO$_x$/NC-200A, MoO$_x$/NC-300A, MoO$_x$/NC-400A, MoO$_x$/NC-500A, MoO$_x$/NC-600A) and 20 wt% Pt/C in 1 M KOH.
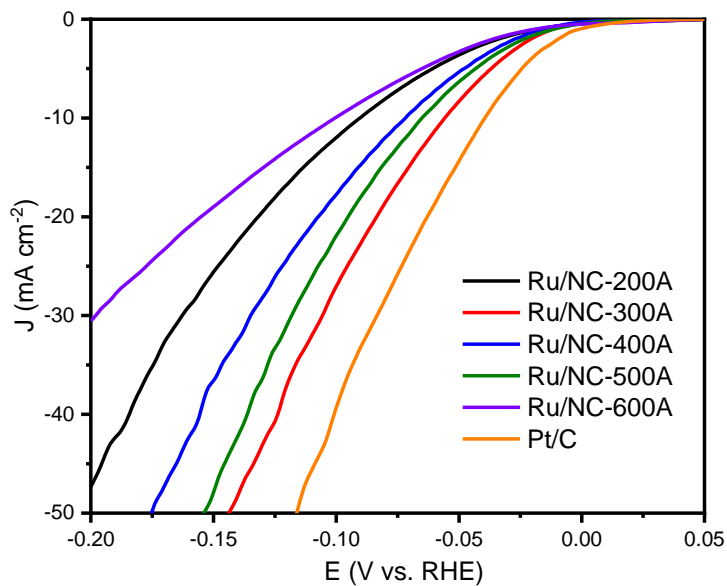
Figure S30. HER polarization curves of Ru/NC composites prepared by MIH at currents varied from 200 A to 600 A for 10 s (i.e., Ru/NC-200A, Ru/NC-300A, Ru/NC-400A, Ru/NC-500A, Ru/NC-600A) and 20 wt% Pt/C in 1 M KOH.
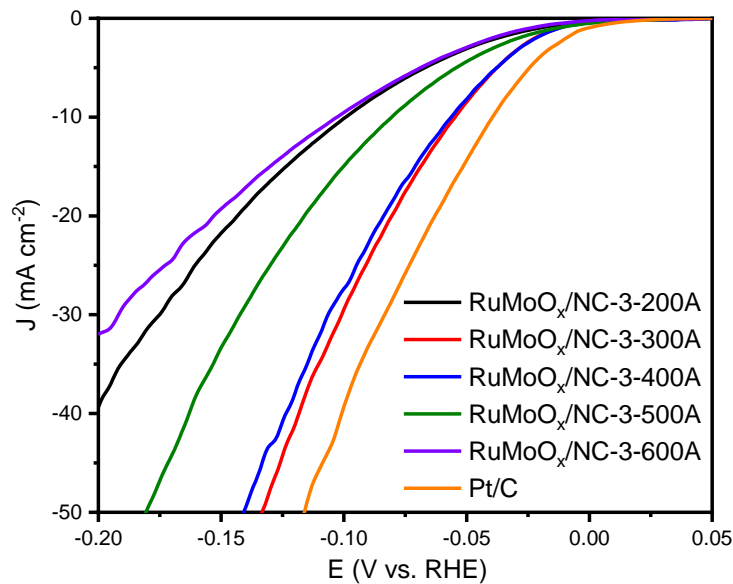
Figure S31. HER polarization curves of $RuMoO_x$/NC composites prepared by MIH at currents varied from 200 to 600 A for 10 s (i.e., $RuMoO_x$/NC-3-200A, $RuMoO_x$/NC-3-300A, $RuMoO_x$/NC-3-400A, $RuMoO_x$/NC-3-500A, $RuMoO_x$/NC-3-600A) and 20 wt% Pt/C in 1 M KOH.

Table S1. Elemental composition (at%) of various samples obtained from SEM elemental mapping.

Sample	C	O	N	Cl	Ru	Mo	Ru+Mo
MoO$_x$/NC	74.7	10.8	10.5	/	/	4.0	4.0
RuMoO$_x$/NC-1	76.2	9.9	10.9	0.5	0.1	2.4	2.5
RuMoO$_x$/NC-2	72.7	10.3	11.5	1.4	1.1	3.0	4.1
RuMoO$_x$/NC-3	76.8	7.4	10.6	2.2	0.9	2.2	3.1
RuMoO$_x$/NC-4	77.2	4.6	11.2	4.2	2.0	0.8	2.8
RuMoO$_x$/NC-5	66.9	10.3	14.2	5.6	2.2	0.8	3.0
Ru/NC	79.0	2.7	10.2	5.0	3.1	/	3.1

Table S2. Elemental composition (at%) of various samples obtained from XPS measurements.

Sample	C	O	N	Cl	Ru	Mo	Ru+Mo
MoO$_x$/NC	77.8	10.67	9.97	/	/	1.55	1.55
RuMoO$_x$/NC-1	81.81	13.15	4.07	/	0.21	0.76	0.97
RuMoO$_x$/NC-2	81.69	14.96	2.28	0.14	0.24	0.68	0.92
RuMoO$_x$/NC-3	83.75	15.23	0.65	0.10	0.15	0.12	0.27
RuMoO$_x$/NC-4	75.04	13.39	5.77	2.13	3.26	0.42	3.68
RuMoO$_x$/NC-5	76.45	11.31	5.67	2.92	3.31	0.34	3.65
RuMoO$_x$/NC-5 etched	77.83	11.98	6.22	0.63	3.18	0.17	3.35
RuMoO$_x$/NC-5 after CV cycles	73.02	21.63	2.45	/	2.45	0.45	2.90
Ru/NC	76.55	12.15	6.36	2.53	2.41	/	2.41

From Table S1, the N contents as evaluated by EDS are very consistent between 10-14 at% among the samples, while in Table S2 (by XPS measurements), the N contents are rather scattered. The discrepancy likely arises from their different probe depth. Results from EDS measurements mostly reflect the material bulk property, whereas XPS is in essence a surface analysis technique.

Table S3. Elemental composition (wt%) of various samples obtained from XPS measurements.

Sample	C	O	N	Cl	Ru	Mo
MoO$_x$/NC	67.05	12.25	10.02	/	/	10.67
RuMoO$_x$/NC-1	73.19	15.68	4.26	/	1.58	5.29
RuMoO$_x$/NC-2	72.74	17.75	2.37	0.37	1.65	5.12
RuMoO$_x$/NC-3	78.22	18.95	0.71	0.28	1.10	0.75
RuMoO$_x$/NC-4	54.90	13.05	4.92	4.60	20.08	2.46
RuMoO$_x$/NC-5	55.45	10.93	4.80	6.25	20.77	1.80
RuMoO$_x$/NC-5 etched	59.28	12.15	5.53	1.42	20.59	1.04
RuMoO$_x$/NC-5 after CV cycles	56.64	22.35	2.22	/	16.00	2.79
Ru/NC	59.40	12.55	5.76	5.80	16.48	/

Table S4. Ru 3p binding energies in the series of samples as determined by XPS measurements.

Sample	Ru^0 (eV)		Ru$^{\delta+}$ (eV)		Zn Auger
RuMoO$_x$/NC-1	462.19	484.39	465.23	487.43	474.54
RuMoO$_x$/NC-2	462.16	484.36	465.21	487.41	474.91
RuMoO$_x$/NC-3	462.08	484.28	465.18	487.38	474.74
RuMoO$_x$/NC-4	462.04	484.24	465.16	487.36	474.56
RuMoO$_x$/NC-5	462.02	484.22	465.14	487.34	474.65
RuMoO$_x$/NC-5 etched	461.99	484.19	465.09	487.29	474.66
RuMoO$_x$/NC-5 after CV cycles	461.80	484.00	464.79	486.99	474.60
Ru/NC	462.01	484.21	465.12	487.32	474.75

Table S5. Mo 3d binding energies in the series of sample as determined by XPS measurements.

Sample	Mo^{4+} (eV)		Mo^{6+} (eV)	
MoO$_x$/NC	229.21	232.31	232.19	235.29
RuMoO$_x$/NC-1	229.50	232.60	232.21	235.31
RuMoO$_x$/NC-2	229.40	233.50	232.24	235.34
RuMoO$_x$/NC-3	229.56	232.66	232.25	235.35
RuMoO$_x$/NC-4	229.75	232.85	232.26	235.36
RuMoO$_x$/NC-5	229.56	232.66	232.33	235.43
RuMoO$_x$/NC-5 after CV cycles	229.03	232.08	232.31	235.35
RuMoO$_x$/NC-5 etched	229.63	232.73	232.29	235.39

Table S6. Fitting results of the EXAFS spectra for the series of samples.

Sample	Peak	σ^2 ($Å^2$)	Distance (Å)	Coordination number
MoO$_x$/NC (73.93% MoO₃, 26.07% MoO₂)	Mo-O	0.0016	1.70	1.5
	Mo-O	0.0104	1.95	3.0
	Mo-O	0.0016	2.30	1.5
	Mo-Mo	0.0069	3.26	1.0
	Mo-Mo	0.0098	3.74	3.0
RuMoO$_x$/NC-1 (84.74% MoO₃, 15.26% MoO₂)	Mo-O	0.0021	1.71	1.7
	Mo-O	0.0077	1.96	2.6
	Mo-O	0.0037	2.28	1.7
	Ru-Ru	0.0019	2.68	5.1
	Mo-Mo	0.0019	3.24	0.6
	Mo-Mo	0.0140	3.75	3.4
RuMoO$_x$/NC-2 (84.74% MoO₃, 15.26% MoO₂)	Mo-O	0.0017	1.70	1.4
	Mo-O	0.0085	1.96	3.2
	Mo-O	0.0016	2.31	1.4
	Ru-Ru	0.0016	2.67	6.2
	Mo-Mo	0.0100	3.21	1.2
	Mo-Mo	0.0066	3.71	2.8
RuMoO$_x$/NC-3 (74.80% MoO₃, 25.20% MoO₂)	Mo-O	0.0016	1.70	1.5
	Mo-O	0.0118	1.95	3.0
	Mo-O	0.0023	2.29	1.5
	Ru-Ru	0.0016	2.68	7.6
	Mo-Mo	0.0056	3.24	1.0
	Mo-Mo	0.0128	3.76	3.0
RuMoO$_x$/NC-4 (77.12% MoO₃, 22.88% MoO₂)	Mo-O	0.0016	1.69	1.5
	Mo-O	0.0177	1.93	2.9
	Mo-O	0.0036	2.29	1.5
	Ru-Ru	0.0016	2.68	8.0
	Mo-Mo	0.0036	3.25	0.9
	Mo-Mo	0.0164	3.76	3.1
RuMoO$_x$/NC-5 (80.51% MoO₃, 19.49% MoO₂)	Mo-O	0.0016	1.70	1.6
	Mo-O	0.0165	1.96	2.8
	Mo-O	0.0017	2.29	1.6
	Ru-Ru	0.0016:	2.68	8.9
	Mo-Mo	0.0026	3.25	0.8
	Mo-Mo	0.0167	3.76	3.2
Ru/NC	Ru-Ru	0.0016	2.68	8.9

Note: The minimum limit for σ is set at 0.04, as only strong bonds can exhibit values smaller than this threshold.

Table S7. Comparison of HER activity in 1M KOH between $RuMoO_x/NC-5$ and other Ru-based HER electrocatalysts.

Electrocatalyst	η_{10} (mV)	Tafel slope (mV dec^{-1})	Reference
$RuMoO_x/NC-5$	-39	28.3	**This work**
Ru/NC-400	-39	40	1
a-RuTe$_2$ PNRs	-41	36	2
Ru-MoS$_2$/CC	-41	114	3
Pd$_3$Ru/C	-42	/	4
MoP-Ru$_2$P/NPC	-47	36.93	5
Ru$_2$P@PNC/CC-900	-50.7	28	6
Ru$_1$CoP/CDs-1000	-51	73.4	7
RuP$_2$@NPC	-52	69	8
Ru/C-H$_2$O/CH$_3$CH$_2$OH	-53	47	9
Ni$_5$P$_4$-Ru	-54	56.7	10
Sr$_2$RuO$_4$	-61	51	11
Ru-Co$_2$P/N-C/NF	-65	65	12
RuNC-2	-81	88	13
S-RuP@NPSC	-92	90.23	14

Table S8. Comparison of charge transfer resistance (R_{ct}, Ω) for the catalysts at various overpotentials.

Sample	$RuMoO_x/NC-1$	$RuMoO_x/NC-2$	$RuMoO_x/NC-3$	$RuMoO_x/NC-4$	$RuMoO_x/NC-5$	Ru/NC
η_{20}	115.7	119.0	105.5	140.6	52.4	132.8
η_{50}	43.2	44.1	39.4	46.3	23.5	45.6
η_{100}	21.2	23.7	20.6	21.5	14.5	24.1

References

1. M. M. Lao, G. Q. Zhao, P. Li, T. Y. Ma, Y. Z. Jiang, H. G. Pan, S. X. Dou and W. P. Sun, *Adv. Funct. Mater.*, 2021, **31**, 2100698

2. J. Wang, L. L. Han, B. L. Huang, Q. Shao, H. L. L. Xin and X. Q. Huang, *Nat. Commun.*, 2019, **10**, 5692.

3. D. W. Wang, Q. Li, C. Han, Z. C. Xing and X. R. Yang, *Appl Catal B: Environ*, 2019, **249**, 91-97.

4. X. P. Qin, L. L. Zhang, G. L. Xu, S. Q. Zhu, Q. Wang, M. Gu, X. Y. Zhang, C. J. Sun, P. B. Balbuena, K. Amine and M. H. Shao, *ACS Catal.*, 2019, **9**, 9614-9621.

5. Y. X. Gao, Z. Chen, Y. Zhao, W. L. Yu, X. L. Jiang, M. S. He, Z. J. Li, T. Y. Ma, Z. X. Wu and L. Wang, *Appl Catal B: Environ*, 2022, **303**, 120879.

6. T. T. Liu, B. M. Feng, X. J. Wu, Y. L. Niu, W. H. Hu and C. M. Li, *ACS Appl. Energy Mater.*, 2018, **1**, 3143-+.

7. H. Q. Song, M. Wu, Z. Y. Tang, J. S. Tse, B. Yang and S. Y. Lu, *Angew. Chem. Int. Ed.*, 2021, **60**, 7234-7244.

8. Z. H. Pu, I. S. Amiinu, Z. K. Kou, W. Q. Li and S. C. Mu, *Angew Chem Int Edit*, 2017, **56**, 11559-11564.

9. Y. Z. Li, J. Abbott, Y. C. Sun, J. M. Sun, Y. C. Du, X. J. Han, G. Wu and P. Xu, *Appl Catal B: Environ*, 2019, **258**, 117952.

10. Q. He, D. Tian, H. L. Jiang, D. F. Cao, S. Q. Wei, D. B. Liu, P. Song, Y. Lin and L. Song, *Adv. Mater.*, 2020, **32**, 1906972.

11. Y. L. Zhu, H. A. Tahini, Z. W. Hu, J. Dai, Y. B. Chen, H. N. Sun, W. Zhou, M. L. Liu, S. C. Smith, H. T. Wang and Z. P. Shao, *Nat. Commun.*, 2019, **10**, 149.

12. Y. Xu, T. L. Ren, K. L. Ren, S. S. Yu, M. Y. Liu, Z. Q. Wang, X. N. Li, L. Wang and H. J. Wang, *Chem Eng J*, 2021, **408**, 127308.

13. Y. T. Li, F. Q. Chu, Y. Liu, Y. Kong, Y. X. Tao, Y. X. Li and Y. Qin, *Chem Commun*, 2018, **54**, 13076-13079.

14. X. Y. Liu, F. Liu, J. Y. Yu, G. W. Xiong, L. L. Zhao, Y. H. Sang, S. W. Zuo, J. Zhang, H. Liu and W. J. Zhou, *Adv Sci*, 2020, **7**, 2001528.